Recent Developments in High-Harmonic Fast Wave Physics in NSTX

B.P. LeBlanc 1), R.E. Bell 1), P. Bonoli 2), R. Harvey 3), W.W. Heidbrink 4), J.C. Hosea 1), S.M. Kaye 1), D. Liu 5), R. Maingi 6), S.S. Medley 1), M. Ono 1), M. Podestà 1), C.K. Phillips 1), P.M. Ryan 6), A.L. Roquemore 1), G. Taylor 1), J.R. Wilson 1) and the NSTX Team

1) PPPL, Princeton, NJ 08543, USA
2) PSFC,-MIT, Cambridge, MA,02139, USA
3) CompX, Del Mar, CA 92014, USA
4) University of California, Irvine, CA 92697, USA
5) Department of Physics, University of Wisconsin-Madison, WI 53706. USA
6) ORNL, Oak Ridge, TN 37831, USA

E-mail contact of main author: leblanc@pppl.gov

Abstract. Understanding the interaction between ion cyclotron range of frequency (ICRF) fast waves and the fast-ions created by neutral beam injection (NBI) is critical for future devices such as ITER, which rely on a combination ICRF and NBI. Experiments in NSTX which use 30 MHz High-Harmonic Fast-Wave (HHFW) ICRF and NBI heating show a competition between electron heating via Landau damping and transit-time magnetic pumping, and radio-frequency wave acceleration of NBI generated fast ions.
Understanding and mitigating some of the power loss mechanisms outside the last closed flux surface (LCFS) has resulted in improved HHFW heating inside the LCFS. Nevertheless a significant fraction of the HHFW power is diverted away from the enclosed plasma. Part of this power is observed locally on the divertor. Experimental observations point toward the radio-frequency (RF) excitation of surface waves, which disperse wave power outside the LCFS, as a leading loss mechanism. Lithium coatings lower the density at the antenna, thereby moving the critical density for perpendicular fast-wave propagation away from the antenna and surrounding material surfaces. Visible and infrared imaging reveal flows of RF power along open field lines into the divertor region.
In L-mode -- low average NBI power -- conditions, the fast-ion D-alpha (FIDA) diagnostic measures a near doubling and broadening of the density profile of the upper energetic level of the fast ions concurrent with the presence of HHFW power launched with $k_{//}$ =-8m^{-1}.
We are able to heat NBI-induced H-mode plasmas with HHFW. The captured power is expected to be split between absorption by the electrons and absorption by the fast ions, based on TORIC calculation. In the case discussed here the T_e increases over the whole profile when ≈2MW of HHFW power with antenna $k_{//}$ =13m^{-1} is applied after the H-mode transition.. But somewhat unexpectedly fast-ion diagnostics do not observe a change between the HHFW heated NBI discharge and the reference NBI only plasma, although an increase in neutron production is measured.

1. Introduction

Understanding the interaction between ion cyclotron range of frequency (ICRF) fast waves and the fast-ions created by neutral beam injection (NBI) is critical for future deuterium-tritium plasma devices such as ITER, which rely on a combination of ICRF and NBI heating to reach a regime dominated by alpha-particle heating. Understanding and mitigating the source of radio- frequency (RF) power loss in the regions outside of the last closed flux surface (LCFS) is equally important. NSTX is a large size spherical torus with a complete set of standard diagnostics, where fast-ion specialized diagnostics like fast-ion D-alpha FIDA [1] are also in operation. It is well suited to study these issues since its auxiliary heating system includes 7-MW NBI and a versatile 6-MW ICRF system. The ion cyclotron harmonic number for the 30 MHz system in NSTX magnetic fields is typically greater than 5 with many resonances present within the plasma. The physics basis of High-Harmonic Fast-Wave (HHFW) heating and a review of recent HHFW research are available elsewhere [2],[3]. Experiments combining HHFW and NBI heating show a competition between two dominant

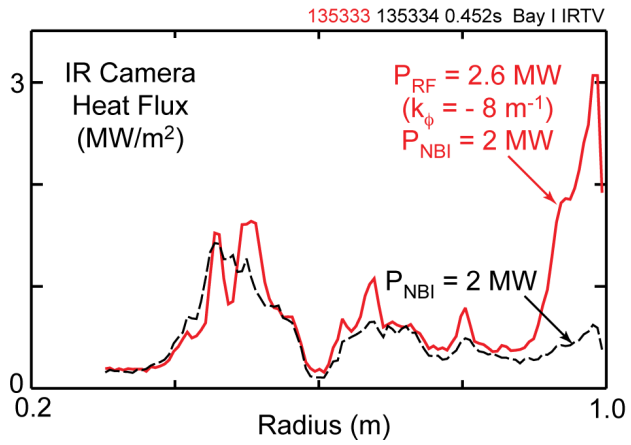

FIG.1. Divertor heat flux vs. major radius: red, HHFW+NBI; black, NBI. (Preliminary calibration). Antenna set to $k_{//}$=-8m^{-1}.

absorption mechanisms inside the last closed flux surface (LCFS) namely: (1) electron heating via Landau damping and transit-time magnetic pumping, and (2) wave-field acceleration of NBI generated fast ions. This paper is organized as follows: Section 2 describes the antenna system and discusses aspects of edge physics relevant to HHFW power coupling. Section 3 describes results obtained with the FIDA diagnostics in L-mode plasmas combining NBI and HHFW heating. Section 4 describes HHFW heating of NBI induced H-mode plasmas and discusses estimates of the amount of power reaching the plasma enclosed within the LCFS. Concluding remarks are presented in Section 5.

2. Antenna, Edge Power Absorption and Dispersion

An array of twelve vertical current elements driven by six 30-MHz transmitters forms a flexible antenna system [4] able to launch toroidally balanced or directed wave spectra characterized by absolute values of $k_{//}$ spanning 3 to 18 m^{-1}. The coupled power typically ranges from 1 to 4 MW, with up to 6 MW possible. Under normal conditions, the radio – frequency (RF) power exiting the antenna travels through the scrape-off layer (SOL) as an evanescent wave until reaching a region where the local electron density is at the critical level for onset of fast-wave propagation perpendicular to the magnetic field. Onset of propagation typically occurs outside of the LCFS, resulting in power being dispersed away from the "confined" plasma by the excitation of surface waves [5]. Infrared light measurements [6] indicate that a significant amount of the antenna power can be redirected to a localized region. Figure 1 shows the heat flux reaching the divertor for two consecutive discharges, both with 2-MW NBI, but with the second having an additional 2.6-MW HHFW heating. In the vicinity of R=1m, the heat flux increases fivefold with RF power applied. Moreover, fast imaging reveals visible light filaments connecting the antenna to the divertor along open field lines. The antenna launch spectrum is co-current directed with $k_{//}$=-8m^{-1}. Edge ion heating by parametric decay instability (PDI) is another phenomenon reducing the power reaching the plasma within the LCFS [7].

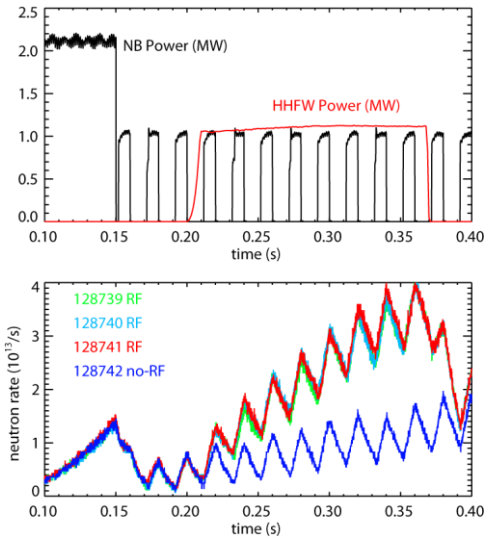

FIG. 2. Top panel: Waveform of injected NB and HHFW power; bottom panel: Measured neutron source strength for three HHFW discharges and one reference plasma.

3. Fast-ion Density Increase with Combined HHFW and NBI Heating of L-mode Plasma

Neutrons produced in NSTX result from nuclear reactions between the fast ions

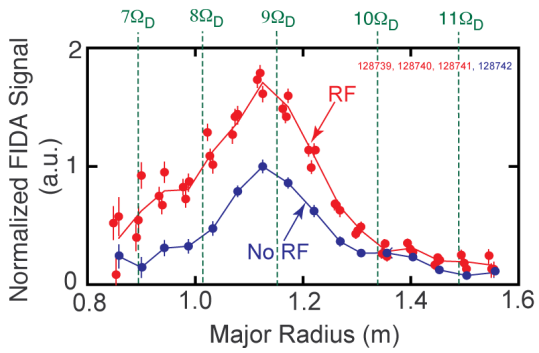

FIG. 3. FIDA signal proportional to fast-ion density profile for discharges with HHFW – labeled as RF – and for the reference plasma. Ion resonance layers are indicated with dotted lines.

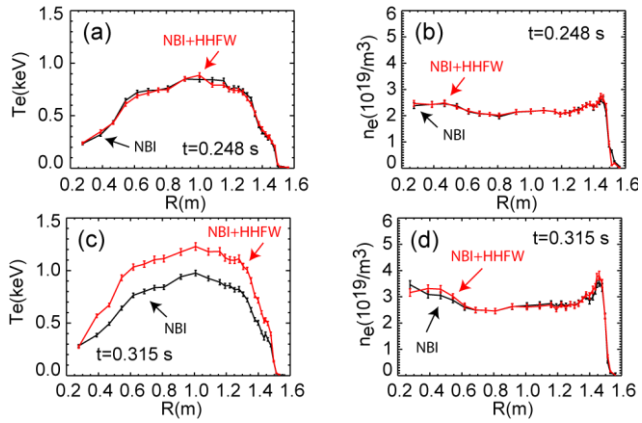

FIG. 4. T_e and n_e profiles just prior and during HHFW heating: Profiles are well matched prior to HHFW onset at t=0.248s -- panels (a) and (b); broad $T_e(R)$ increase during HHFW heating at t= 0.315s, while $n_e(R)$ remains matched, panels (c) and (d).

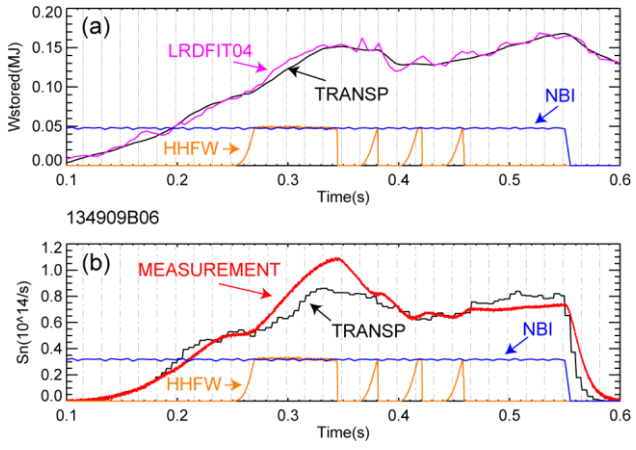

FIG. 5. (a) Time overlay of LRDFIT stored energy with TRANSP output; (b) Neutron production S_n compared to TRANSP prediction.

generated by NBI and the target plasma thermal ions. The neutron source strength, S_n, typically increases during HHFW heating of NBI-induced L-mode plasma [8]. A series of discharges have been designed to measure the fast-ion density profile using the FIDA diagnostic. Fig.2 shows the time variation of the NBI and HHFW power into the target plasmas. HHFW power of 1MW, with antenna launch spectrum of $k_{//}=8m^{-1}$, is applied during a series of NBI pulses at 65KV. An NBI-only reference discharge was also obtained. A cumulative rise of the neutron production results in a near tripling of S_n compared to the reference discharge. We can see in Fig.3 an overlay of the profile of the "FIDA signal", which, in this analysis, is proportional to the density of high-energy fast ions. In this case, the FIDA spectra are integrated over energies ranging from 30keV to 60keV. One can see a near doubling of the fast-ion density and a broadening when HHFW is added to NBI. The ion resonance layers range from the 7th to the 11th harmonic of deuterium. More information can be found elsewhere [9,10].

4. HHFW Heating of NBI-induced H-mode plasma

Of particular interest for the NSTX research program is the application of HHFW heating to NBI-induced H-mode plasmas in order to enhance high performance discharges. In the past this task has proved challenging, with essentially no HHFW power reaching the plasma within the LCFS [11]. Recently, we were able to couple a sizeable amount of power to the enclosed plasma resulting in a significant increase in the total stored energy and in the neutron rate. Benign MHD activity was observed in these discharges. Moreover, $T_e(R)$ increased over essentially the whole radial profile. Figure 4 shows Thomson scattering T_e and n_e profile overlays from a discharge with combined NBI and HHFW heating and a reference

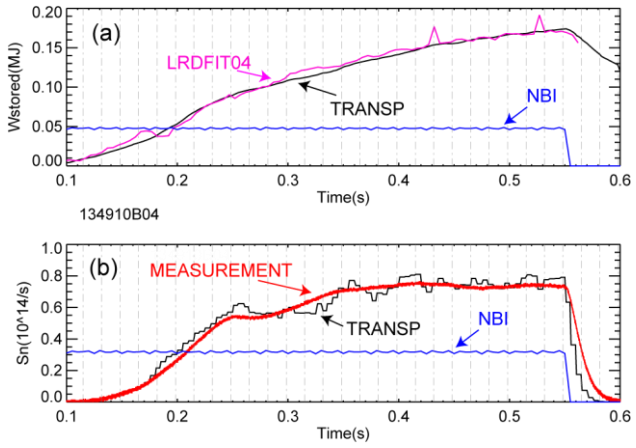

FIG. 6. (a) Time overlay of LRDFIT stored energy with TRANSP output; (b) Neutron production S_n compared to TRANSP prediction.

NBI-only plasma. In panels (a) and (b) we can see that T_e and n_e profiles are well matched at t=0.248s, prior to the HHFW heating onset, commencing at 0.25s. One also sees from the steep n_e gradient measured at the outer edge that the plasma is in H mode prior to start of HHFW heating. Panel (c) shows the $T_e(R)$ overlay at t=0.315s during HHFW heating: T_e increases over the whole profile except for the innermost and outermost radial measurements; the n_e profiles remain in H mode and well matched as can be seen in panel (d). The two discharges were generated consecutively. This data provides clear indication of electron heating. We can see in Fig.5(a) a temporal overlay of the experimental total stored energy, W_{stored} obtained from LRDFIT[12] equilibrium reconstructions, compared with a W_{stored} estimate from TRANSP[13]. Power traces – not to scale -- show the 2-MW NBI and 2.0-MW HHFW power time evolution. The antenna phasing is set for a spectrum characterized by $k_{//}$ =13m^{-1}. The plasma current is 0.9MA and the toroidal field is 0.55T. There is a good agreement between the total stored energy from LRDFIT and TRANSP. A similar plot is shown in Fig.5(b) for the neutron time source strength S_n. Currently TRANSP utilizes a version of the full-wave code TORIC [14] able to compute the power deposition under high-harmonic conditions, but unfortunately the software needed to evolve self-consistently the fast-ion energy distribution under the influence of wave field is not available. TRANSP uses the measured T_e profile, but the estimated S_n reflects the beam-target reactions for the fast-ions generated by NBI without acceleration by HHFW. For reference we show in Fig.6 results for the well matched NBI-only discharge mentioned above. One can see that in the absence of HHFW power, TRANSP reproduces well the stored energy and the neutron production rate. In these calculations, TRANSP uses equilibria from LRDFIT, but some uncertainty remains about the q profile since the MSE [15] diagnostic was not available for this discharge. The q profile of the LRDFIT equilibrium reconstructions used here are in better agreement than those obtained with EFIT [16] for another similar discharge taken the same day, for which MSE was available. The discrepancy between the measured neutrons and the TRANSP estimate for the NBI+HHFW discharge will be discussed below in more detail.

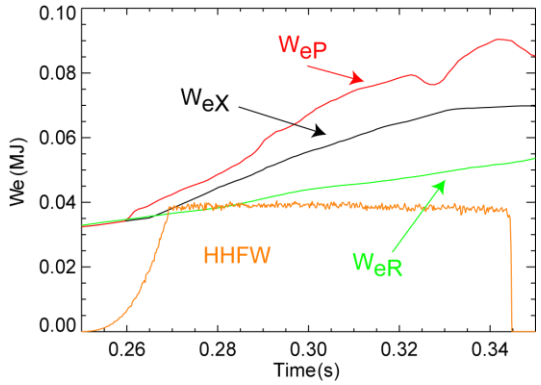

FIG.7: Time evolution of electron stored energy: W_{eX}, NBI+HHFW plasma; W_{eP}, predicted from TORIC and χ_e from reference plasma; W_{eR}, reference NBI-only plasma. Unscaled HHFW power trace.

As discussed earlier, part of the power launched from the antenna is absorbed in the SOL, while the remaining fraction reaches the enclosed plasma. The power absorbed in the SOL is quickly lost to the first wall, in particular in the divertor region as seen in Fig.1. In the following, we estimate the amount of power reaching the confined

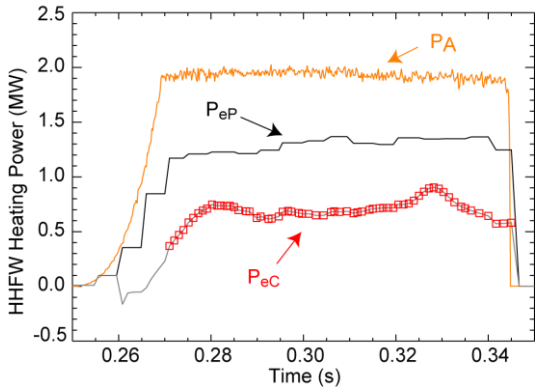

FIG. 8. HHFW electron heating power allotment: Antenna power, P_A; TORIC prediction of power absorbed by electrons assuming 100% coupling, P_{eP}; estimated power coupled to electrons, P_{eC}

plasma based on the increase of the electron stored energy observed during HHFW heating. We make use of three TRANSP calculations of the electron stored energy: (1) the analysis based on the experimental data for combined NBI and HHFW heating, which is shown in Fig.5; (2) the analysis based on the NBI-only experimental data, which is shown in Fig.6; (3) a predictive TRANSP calculation in which the electron thermal diffusivity, χ_e, from the NBI-only reference discharge is used to predict T_e for the combined NBI and HHFW heating scenario using TORIC's HHFW power deposition calculation and assuming that 100% of the antenna power reaches the enclosed plasma. We can see in Fig.7 an overlay of the time evolution for these three cases, where W_{eX} is the electron stored energy obtained from the experimental NBI+HHFW TRANSP analysis, W_{eR} corresponds to the reference NBI-only analysis, and W_{eP} corresponds to the predictive calculation mentioned above. There is a good match for times prior to the HHFW pulse onset, but later on W_{eP} exceeds W_{eX}. W_{eR} is needed in order to compensate for the electron stored energy increase in absence of HHFW power.

Figure 8 shows the time evolution of the HHFW power P_A launched from the antenna, ≈1.9 MW is launched. The figure also shows P_{eP}, the power absorbed by the electrons as computed by TORIC and assuming that all the antenna power reaches within the LCFS. The power coupled to the enclosed plasma is computed as $P_{eC} = f_C \times P_{eP}$, where the fraction, f_C, of the antenna power captured within the enclosed plasma is estimated using the ratio $f_C=(W_{eX}-W_{eR})/(W_{eP}-W_{eR})$. The evaluation is done for times when the P_{eP} is greater than 1MW and is indicated by the square symbols. One gets a set of values characterized by an average of $\langle f_C \rangle = 0.53 \pm 0.07$, where the latter is the standard deviation. Similarly for P_{eC}, one gets $\langle P_{eC} \rangle$ = 0.7MW with a standard deviation of 0.1MW.

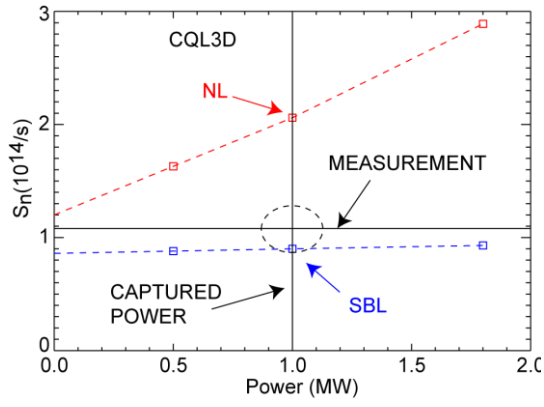

FIG. 9. CQL3D HHFW power S_n scan: red squares, NL calculation, blue squares, SBL calculation. Horizontal line, measurement. Vertical line, estimate of HHFW power deposited into fast ions. Dashed oval indicates range of uncertainty.

Using the coupling coefficient $\langle f_C \rangle$ to estimate how much of the 1.9MW power leaving the antenna is absorbed within the enclosed plasma, one gets that 0.53*1.9=1.0MW±0.13MW is captured within the LCFS. Of this captured power, 0.7MW is absorbed by the electrons as we have seen above, leaving 0.3 ±0.1MWfor the fast ions, where the error was carried from the P_{eC} evaluation above. We have used the code CQL3D [17] to compute the effects of HHFW acceleration on the fast ions and its effects on the neutron production. In its current version, CQL3D offers two options for the evolution of the fast-ion distribution: (1) the "no loss" option (NL), which assumes zero banana width orbits; (2) the "simple-banana-loss"

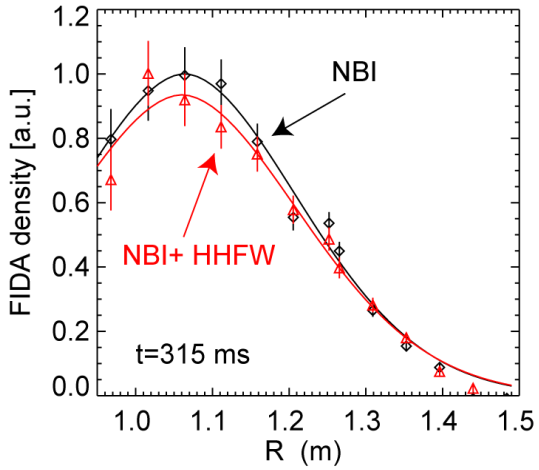

FIG. 10. FIDA density profiles at t=0.315s for, red, plasma with NBI+HHFW heating and, black, reference NBI-only plasma.

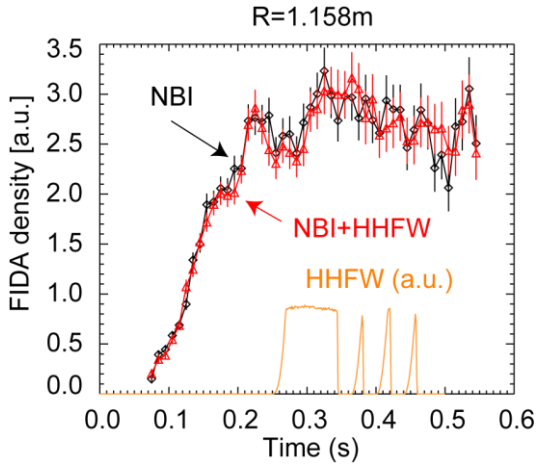

FIG. 11. Evolution at R=1.158m of FIDA density for, red, plasma with NBI+HHFW and, black, reference NBI-only plasma.

calculation (SBL), which assumes that trapped ions with a banana width plus gyro radius greater than the distance to the outer flux surface are lost in one bounce time. Using input profiles and equilibrium data from TRANSP at a particular time of interest, CQL3D is "run to equilibrium" in order to get an estimate of the neutron rate enhancement resulting from HHFW heating. While the NL calculation will overestimate the neutron rate, the SBL calculation should underestimate the S_n since it assumes that the LCFS is equivalent to a fuzzy first wall. We can see in Fig.9 results from a power scan calculation, where both NL and SBL fast-ion calculations are used to estimate the neutron production rate for time t=0.34s. The experimental value is indicated by a horizontal line. The 1.0MW captured power mentioned above is shown as a vertical line. As expected, the NL predictions exceed the experimental value. On the other hand the SBL calculations show a weak power dependency and underestimate the neutron measurement. The dotted oval corresponds to the uncertainty based on the HHFW captured power estimate mentioned above 1.0 ± 0.13MW and the S_n experimental error of 20%. On the other hand, the fast-ion diagnostics FIDA and neutral particle analyzer NPA [18] do not detect measurable change between the combined NBI+HHFW and the NBI-only plasma in this case. One can see in Fig. 10 an overlay of the FIDA profiles for the combined NBI and HHFW discharge and for the reference NBI-only plasma at t=0.315s, which is the later time displayed in Fig.4. The data are normalized to the maximum point of the reference discharge. Within experimental error, the two profiles are the same: peaked and centered near R=1.06m. We also show in Fig.11 the time evolution of the FIDA density at R=1.158m for the NBI+HHFW and NBI discharges. Again, no net change can be observed between the NBI+HHFW and NBI only discharges. The FIDA data shown here is representative of fast ions with an energy ranging from 15KV to the NBI injection energy of 90KV. Hence the experimental observation suggests that no or very little HHFW power is noticeably modifying the fast-ion distribution in the phase space covered by FIDA and NPA. The neutron production

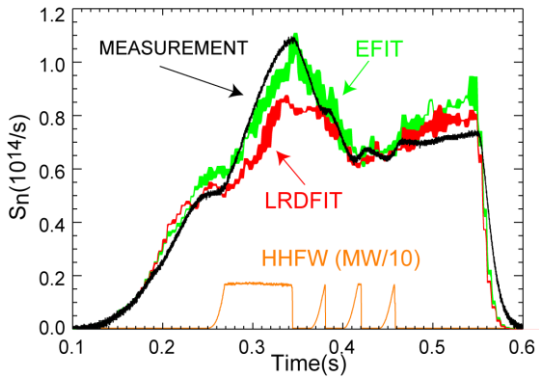

FIG.12. Overlay TRANSP S_n prediction when using equilibrium from, red, LRDFIT and from, green, EFIT.

enhancement occurring during HHFW heating can be caused by three effects: (1) the $T_e^{3/2}$ scaling of the beam-target neutron generation [19]; (2) the HHFW field acceleration of fast ions; (3) a peaking of the current profile occurring during HHFW heating. As mentioned earlier, the T_e effects on the beam-target production are folded into the TRANSP analysis, but not the fast-ion acceleration. Moreover, the current profile in TRANSP depends on the equilibrium imposed on its calculations. We can see in Fig.12 a time overlay of the measured neutrons compared with TRANSP predictions based on LRDFIT equilibrium and EFIT equilibrium. As mentioned above, we chose to use LRDFIT because it resulted in a better match to a similar plasma with MSE measurement on the same day. But it is noteworthy that the EFIT based TRANSP analysis produces a better match to the measured neutrons. The reason behind this difference could be that the central q is lower or equivalently the plasma current profile is more peaked when using EFIT. More current in the core region is conducive to better fast-ion confinement and higher neutron production. This observation illustrates the need for MSE measurement for future experiments. Lithium coating of the first wall [20] has helped to lower the density in front of the antenna and move the onset layer away from the antenna and first wall, and hence reducing SOL losses. We show in Fig.13 Thomson scattering measurements of the density R=1.562m or about 0.015m in front of the antenna and an estimate of the onset density for the NBH+HHFW discharge discussed above. One can see that n_e remains lower than the onset density during the HHFW pulse.

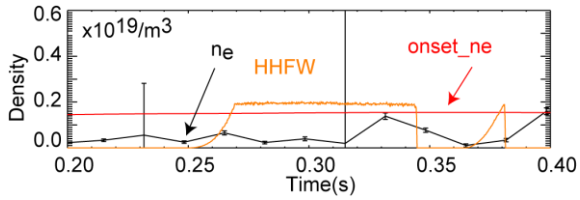

FIG.13. Electron density and onset density at R=1.562m.

5. Conclusion

Recent work has been focused on the optimization of the coupling of HHFW power to the enclosed plasma, with special attention to discharges with NBI. A near doubling of the density profile of the higher-energy fraction of the fast ions has been measured with FIDA, corresponding to the HHFW acceleration of NBI induced fast particles. The plasmas in this study had low NBI average power and remained in the L mode. HHFW heating of NBI-induced H-mode plasmas has been observed on many occasions. The improved coupling is partly attributed to the Lithium first wall coating. Thomson scattering measurements indicate that the electron temperature can increase over most of the radial profile. Analysis of a discharge where HHFW power is applied to the plasma after it had undergone an H-mode transition has been conducted. TRANSP/TORIC analyses reveal that about half of the antenna power is captured within the LCFS: about two thirds of it is absorbed by the electron and one third by the fast ions. On the other hand fast-ion diagnostics FIDA and NPA were not able to observe a difference between the NBI+HHFW plasma and the reference discharge. This result differs from previous experience at higher plasma current, where NPA observed the formation of a tail; further work is needed to understand this behavior. Localized power flux in the low MW/m^2 has been observed during HHFW heating by infrared radiation measurement. This work is supported by DOE DE-AC02-09CH11466.

[1] M. PODESTA, W. W. Heidbrink, R. E. Bell, and R. Feder, Rev. Sci. Instr., 78, 10E521 (2008)
[2] M. ONO, Physics of Plasmas, **2**, (1995) 4075
[3] G. TAYLOR, et al., Physics of Plasmas, Vol. 17 (2010) 056114
[4] J.R. WILSON *et al.*, Phys. Plasmas, **10**, No. 5, (2003) 1733

[5] J.C. HOSEA, *et al*., Phys. Plasmas **15** (2008) 056104
[6] D.M. MASTROVITO, et al., Rev. Sci. Instrum. 74 (2003) 5090
[7] T.BIEWER, *et al*, Phys. of Plasmas **12** (2005) 056108
[8] A.L. ROSENBERG, *et al*, Phys. of Plasmas 11 (2004) 2441-2452
[9] D. LIU, at 1l. Plasma Physics and Controlled Fusion, Vol. 52 (2010) 025006
[10] M. PODESTA, et al., Radio Frequency Power in Plasmas, AIP Conf. Proc. 1187 (2009) 69-76
[11] B.P. LEBLANC, *el al*, Radio Frequency Power in Plasmas, AIP Conf. Proc. 787 (2005) 86
[12] J.E. MENARD, *et al.*, PRL **97,** 095002 (2006)
[13] R.J. HAWRYLUK, Physics of Plasma Close to Thermonuclear Conditions, CEC/Pergamon, Brussels, 1980,Vol. 1, p. 19
[14] M. BRAMBILLA, Plasma Phys. Control. Fusion **44** (2002) 2423
[15] F.M. LEVINTON, H. YUH, Rev. Sci. Instrum. **79**, (2008) 10F522
[16] S.A. SABBAGH, S.M. KAYE, J.E. MENARD, et al., Nucl. Fusion **41** (2001) 1601
[17] R. HARVEY, USDOC/NTIS No. DE93002962 (1992); (http://www.compxco.com/cql3d.html)
[18] S.S. MEDLEY, et al., Nuclear Fusion, Vol. 44 (2004) 1158-1175
[19] H.W. HENDEL, et al., Journal of Fusion Energy, Vol. 5 (1986) 231-244
[20] M. G. BELL, et al., Plasma Phys. Controlled Fusion **51**, (009) 124054